Marine biodiversity exposed to prolonged and intense subsurface heatwaves

🔴 Check for updates

Eliza Fragkopoulou ⬤ [1] ✉, Alex Sen Gupta ⬤ [2,3], Mark John Costello ⬤ [4], Thomas Wernberg ⬤ [5,6], Miguel B. Araújo ⬤ [7,8], Ester A. Serrão ⬤ [1], Olivier De Clerck[9] & Jorge Assis ⬤ [1,4] ✉

Marine heatwaves (MHWs) are becoming increasingly common, with devastating ecosystem impacts. However, MHW understanding has almost exclusively relied on sea surface temperature with limited knowledge about their subsurface characteristics. Here we estimate global MHWs from the surface to 2,000 m depth, covering the period 1993–2019, and explore biodiversity exposure to their effects. We find that MHWs are typically more intense in the subsurface at 50–200 m and their duration increases up to twofold with depth, although with large spatial variability linked to different oceanographic conditions. Cumulative intensity (a thermal stress proxy) was highest in the upper 250 m, exposing subsurface biodiversity to MHW effects. This can be particularly concerning for up to 22% of the ocean, where high cumulative intensity overlapped the warm range edge of species distributions, thus being more sensitive to thermal stress. Subsurface MHWs can hence drive biodiversity patterns, with consequent effects on ecological interactions and ecosystem processes.

The frequency and duration of marine heatwaves (MHWs) have been increasing over the past century[1–3] and are anticipated to further increase in the decades to come[4], driven by anthropogenic climate change and ocean warming[1,2,5]. MHWs have caused substantial biological[6,7] and socio-ecological[8] impacts globally, ranging from rapid shifts in species distributions to mass mortality of marine organisms[8–10]. To date, MHWs have been studied primarily at the ocean surface due to the availability of high-quality sea surface temperature datasets[9], and only a few studies, all based on individual locations or events, have examined MHWs throughout the water column[10–18]. These studies focused on sites with long-term mooring data[16,17], or individual strong long-lasting MHWs partially resolved using Argo data[11,13,14], or ocean models[12,15,18]. A global assessment of MHW spatial and temporal depth structure is still missing, hindering the examination of commonalities and differences across regions.

Localized observations have shown greater MHW intensity in the subsurface[11,13,16,17], with warming persisting for up to two years after the end of surface events[19]. Several processes can affect the depth structure of MHWs. In the northeastern Pacific, salinity differences impacting the water column stratification determined the depth extent of warming during two distinct MHW events[13]. The enhanced stratification in 2019–2020 restricted the warming from extending as deep as in the 2013–2016 event[13]. In the tropical western Pacific, subsurface MHWs were related to Ekman convergence and downwelling of warm surface waters[17]. In southeastern Australia, local downwelling also caused subsurface warming, at times without a surface signal[11,16]. In the northwestern Atlantic, subsurface MHWs were driven by warm core rings spinning off the Gulf Stream boundary current over the slope and shelf region, and were decoupled from surface events[18].

[1]CCMAR – Centre of Marine Sciences, University of Algarve, Faro, Portugal. [2]Climate Change Research Centre, University of New South Wales, Sydney, New South Wales, Australia. [3]Australian Research Council Centre of Excellence for Climate Extremes, University of New South Wales, Sydney, New South Wales, Australia. [4]Faculty of Biosciences and Aquaculture, Bodø, Norway. [5]UWA Oceans Institute & School of Biological Sciences, University of Western Australia, Crawley, Western Australia, Australia. [6]Norwegian Institute of Marine Research, Flødevigen Research Station, His, Norway. [7]Department of Biogeography and Global Change, National Museum of Natural Sciences, CSIC, Madrid, Spain. [8]Rui Nabeiro Biodiversity Chair, MED – Mediterranean Institute for Agriculture, Environment and Development, University of Évora, Évora, Portugal. [9]Phycology Research Group, Biology Department, Ghent University, Ghent, Belgium. ✉e-mail: eli_frag@hotmail.com; jorgemfa@gmail.com

Given that MHW intensity may be stronger below the surface[11,13,16,17], a global characterization of subsurface MHWs could improve understanding of their potential impacts on marine biodiversity[9,20]. In this Article, we advance this understanding by using global high-resolution (1/12°) reanalysis temperature data[21] from 1993 to 2019 at 11 depths (0, 25, 50, 75, 100, 150, 200, 250, 500, 1,000 and 2,000 m), validated against in-situ observations (Supplementary Information), to estimate MHW metrics per depth and over time. Further, we provide novel insights into the potential biodiversity exposure to MHWs globally by overlaying the spatial distribution of cumulative MHW intensity with species richness estimates[22] derived from the modelled ranges of 25,078 species distributed from the surface to 2,000 m[23].

Global MHW metrics with depth

Temperature reanalysis data from 1993 to 2019 showed multi-decadal warming of the global ocean, with a stronger signal above 500 m (Fig. 1a). In the upper 100 m, warming was modulated by strong interannual variability, such as the extreme 1997/1998 and 2016/2017 El Niño events[24], whose impacts become lagged with depth. The progressive warming of the global ocean expanded in depth, reaching 1,000 m over recent years, with a lack of cold temperature anomalies after 2015 (Fig. 1a). The reanalysis and in-situ data showed a good agreement (Supplementary Table 2), yet temperature estimates from the deep ocean, polar latitudes, ice-covered regions and prior to 2004, when subsurface Argo float data measurements were less widespread, should be interpreted with caution because they are highly uncertain (Methods).

The global average MHW maximum intensity, that is, the average of the maximum temperature anomaly from the climatology of each MHW event, remained greater than 1.3 °C in the upper 200 m of the ocean (Fig. 1). Remarkably, the highest intensity was found at 100 m depth with a mean ± s.d. of 1.6 ± 1.0 °C. This was 19% higher than surface events (1.3 ± 0.5 °C; Fig. 1 and Supplementary Table 3). Even at 200 m depth, the intensity was still as high as at the surface (1.3 ± 0.8 °C). Deeper than 200 m, global MHW intensity typically reduced with depth, decreasing to 0.37 ± 0.28 °C at 1,000 m and 0.15 ± 0.09 °C at 2,000 m depth (Fig. 1 and Supplementary Table 3). This global pattern of subsurface MHW intensification could be related to vertical displacements of the thermocline, the upper ocean layer characterized by a steep temperature gradient with depth (Fig. 1f), resulting in warmer temperatures at fixed depths[11,13,16,17].

The globally averaged occurrence of MHWs, that is, the number of individual events from 1993 to 2019, decreased with depth, from an average of 44 ± 10 events at the surface to 28 ± 11 events at 2,000 m depth (Fig. 1 and Supplementary Table 3). Conversely, the average duration of MHW increased twofold, from 20 ± 6 days at the surface to 40 ± 19 days at 2,000 m depth (Fig. 1 and Supplementary Table 3). Notably, both metrics showed little variation between 50 and 250 m depth.

The sum of cumulative intensity, that is, the integral of MHW intensity over the duration of each event[25] (in °C days; Fig. 1e), was estimated as a proxy of thermal stress. This ranged from an average of 1,007 ± 435 °C days at the surface to 141 ± 92 °C days at 2,000 m (Supplementary Table 3). Like the intensity pattern, the highest average cumulative intensity was at 100 m depth with a mean of 1,439 ± 849 °C days. At 500 m, MHW cumulative intensity decreased to almost half that at the surface and continued to decrease in deeper waters, despite the increase in MHW duration (Fig. 1 and Supplementary Table 3).

Time series analyses of temperature anomalies revealed strong synchrony between surface and subsurface layers down to 50 m depth (correlation 0.75 ± 0.24; Supplementary Table 3), decreasing rapidly from the surface to 100 m and more slowly subsequently, yet with large variability (Fig. 1g). The increased synchrony in the upper 100 m is to be expected, as this represents the typical mixed layer depth within which water mass homogenization occurs[26]. Below the mixed layer, reduced synchrony in warming indicates disassociated processes of surface and subsurface temperature variability and therefore potentially disassociated MHW drivers.

Spatial patterns of MHWs

Spatial variations in MHW metrics prevailed across depths (Fig. 2). The strongest and most frequent MHWs were primarily observed in regions of sharp temperature gradients, such as those associated with boundary currents and fronts. However, these events tended to have a short duration (Fig. 2). For example, in the Gulf Stream (northwestern Atlantic Ocean) and Agulhas Current (South Indian Ocean) extensions, frequent and strong MHWs were detected as deep as 1,000 m (Fig. 2), matching the depth extension of the boundary currents[27]. Strong MHWs also occurred in regions along the Equator but in the subsurface (for example, 100 m depth; Fig. 2). The longest MHW durations were often estimated in polar regions (for example, the Weddell Sea in the Antarctic), a pattern that was replicated down to the maximum depth (Fig. 2). At 2,000 m, prolonged MHWs were common in every ocean basin (Fig. 2).

Biodiversity exposure to MHWs

We used MHW cumulative intensity (°C days) and species distributions to estimate biodiversity exposure to MHWs. In this context, we defined richness exposure as the overlap of cumulative intensity and species richness[22], that is, the number of species in each cell (Fig. 3). Because thermal tolerances are more easily exceeded at the warm range edge of species distributions[6], we used warm-edge exposure as a proxy of thermal sensitivity and define it as the overlap of cumulative intensity and warm-edge richness, that is, the number of species at the warm range edge of their distributions in each cell (Fig. 3 and Supplementary Fig. 8). Regions of highest/least exposure were defined where high richness overlayed high/low cumulative intensity.

Overall, regions of highest richness exposure varied across depths (Fig. 3), depending on MHW cumulative intensity and species richness estimates, with both being greater in the upper 250 m of the ocean (Supplementary Table 4). Averaged across depths, 14% of the ocean was classified as high richness exposure, ranging between 11% at the surface and 250 m depth and 16% at 75 and 100 m depth (Fig. 3 and Supplementary Table 4). Despite spatial variability, some regions were recurrently classified as high richness exposed across depths, such as in the Philippine and Tasman seas (West Pacific), the Gulf of Mexico (North Atlantic) and off South Africa in the South Indian Ocean. In contrast, regions of least richness exposure represented a smaller portion of the ocean, 8% on average, ranging between 6% (for example, equatorial Pacific at 500 m depth) and 11% (for example, surface tropical Atlantic). Highest warm-edge exposure comprised an average of 15% of the global ocean across depths, ranging from only 6% at the surface to up to 22% at 1,000–2,000 m depth, comprising large portions of the Indian and North Atlantic oceans (Fig. 3 and Supplementary Table 5). Regions such as the Gulf of Mexico, the Gulf of Aden and the Tasman Sea were consistently classified as highly exposed across depths, both for richness and warm-edge exposure, being of particular concern for potential biological effects. In contrast, regions classified as least warm-edge exposed represented on average 8% of the ocean, ranging from 3% at 500 m (for example, North Indian Ocean) to 17% at the surface (for example, tropical Atlantic and Indian oceans; Fig. 3 and Supplementary Table 5).

Local MHW and biodiversity patterns

Local time–depth analyses of maximum MHW intensity and biodiversity metrics were produced for selected locations with distinct oceanographic or climatic conditions. Different patterns in the intensity, frequency, duration and depth extent of MHW events emerged, depending on the prevailing conditions (Fig. 4 and Extended Data Figs. 1 and 2). In regions of boundary currents and fronts (Fig. 4a,b and Extended Data Fig. 1a,b), MHWs typically extended at depths well
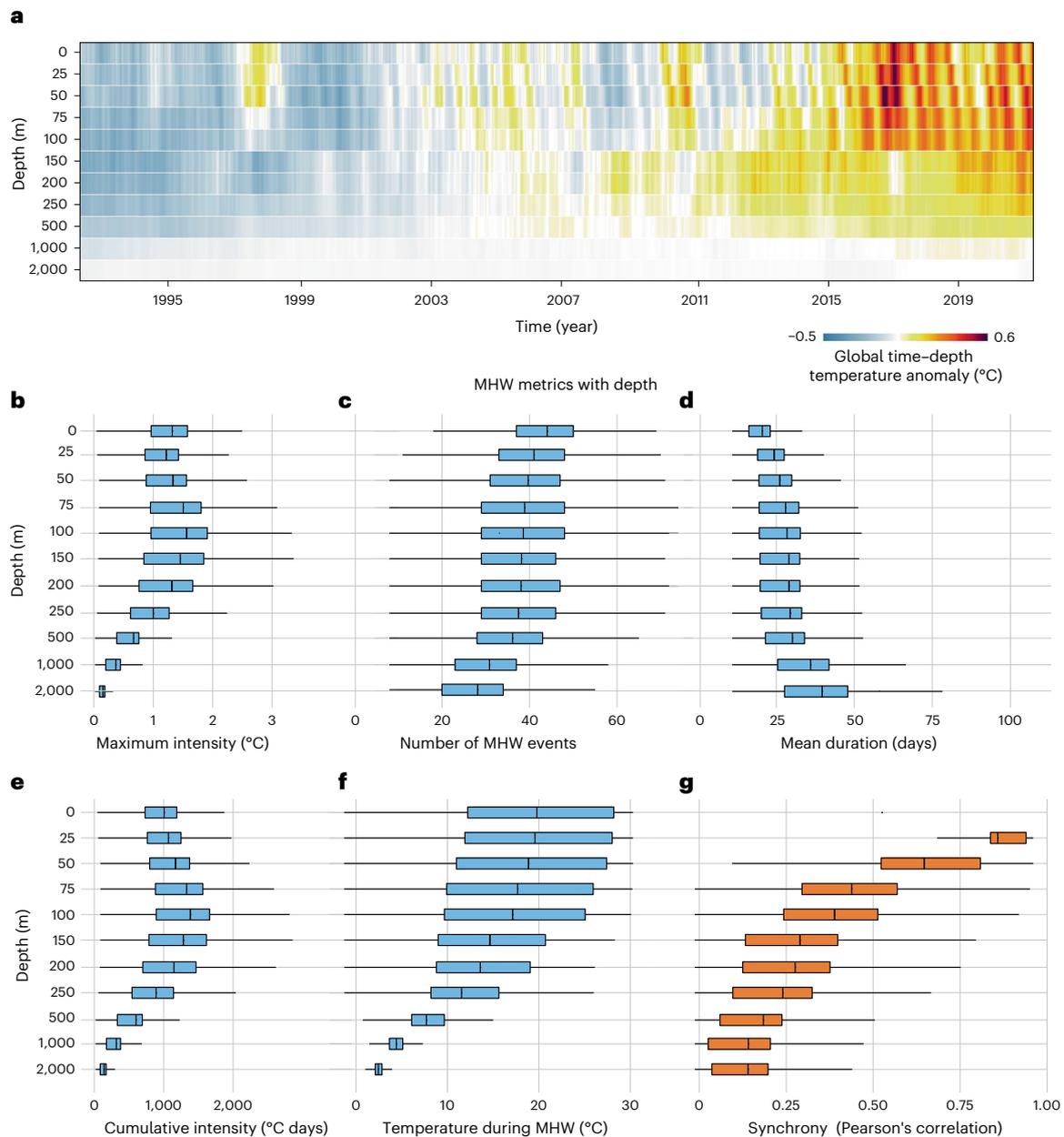
Fig. 1 | Global MHW metrics from the surface to 2,000 m for the period 1993–2019. a, Time–depth global average temperature anomalies at each depth (levels not to scale). **b**–**f**, Global average estimates of MHW maximum intensity (**b**), occurrence (**c**), duration (**d**), cumulative intensity (**e**) and ocean temperature (**f**) during maximum MHW intensity, for each depth. (**g**) Temporal correlation of temperature anomalies between the surface and subsurface levels (95% confidence level). The boxplot central line represents the mean, edges the 25th and 75th percentile, and whiskers the 5th and 95th percentile of values (n = 31,073 cells). Outliers are not shown but full range values are presented in Supplementary Table 3.

below the thermocline, reaching down to 1,000 m (Supplementary Fig. 9a,b). Under these conditions, MHWs had a short duration, and the highest (cumulative) intensity was typically found from the surface to 500 m depth. In regions of subtropical gyres (Fig. 4c and Extended Data Fig. 2c), MHWs tended to last longer, and higher MHW (cumulative) intensities were found from the surface to the thermocline depth (Supplementary Fig. 9c), where they often peaked. Weaker-intensity MHWs also occurred below the thermocline, at times unconnected to surface events. In regions of tropical gyres (Fig. 4d and Extended Data Fig. 2d), subsurface MHWs were predominantly unconnected to the surface and had shorter durations. The highest intensities were estimated in the subsurface at the thermocline depth (Supplementary Fig. 9d). In the Arctic (Fig. 4e and Extended Data Fig. 2e),

subsurface MHWs were particularly prolonged (up to three years) and appeared to be mostly unconnected to the surface. They primarily occurred below the thermocline depth (Supplementary Fig. 9e), where cumulative intensity peaked despite the higher intensities found at the surface. Regional biodiversity patterns of species and warm-edge richness varied greatly among regions and depths, ranging from species richness of over 400 in the subtropical South Atlantic to less than 10 in the Arctic, with a richness increase in deeper demersal communities (Fig. 4 and Extended Data Fig. 2). The highest exposure to MHW effects, estimated in depths where richness and cumulative intensity were the greatest, was between 50 and 100 m depth across all regions except for boundary currents, where exposure peaked deeper, at 250–500 m.
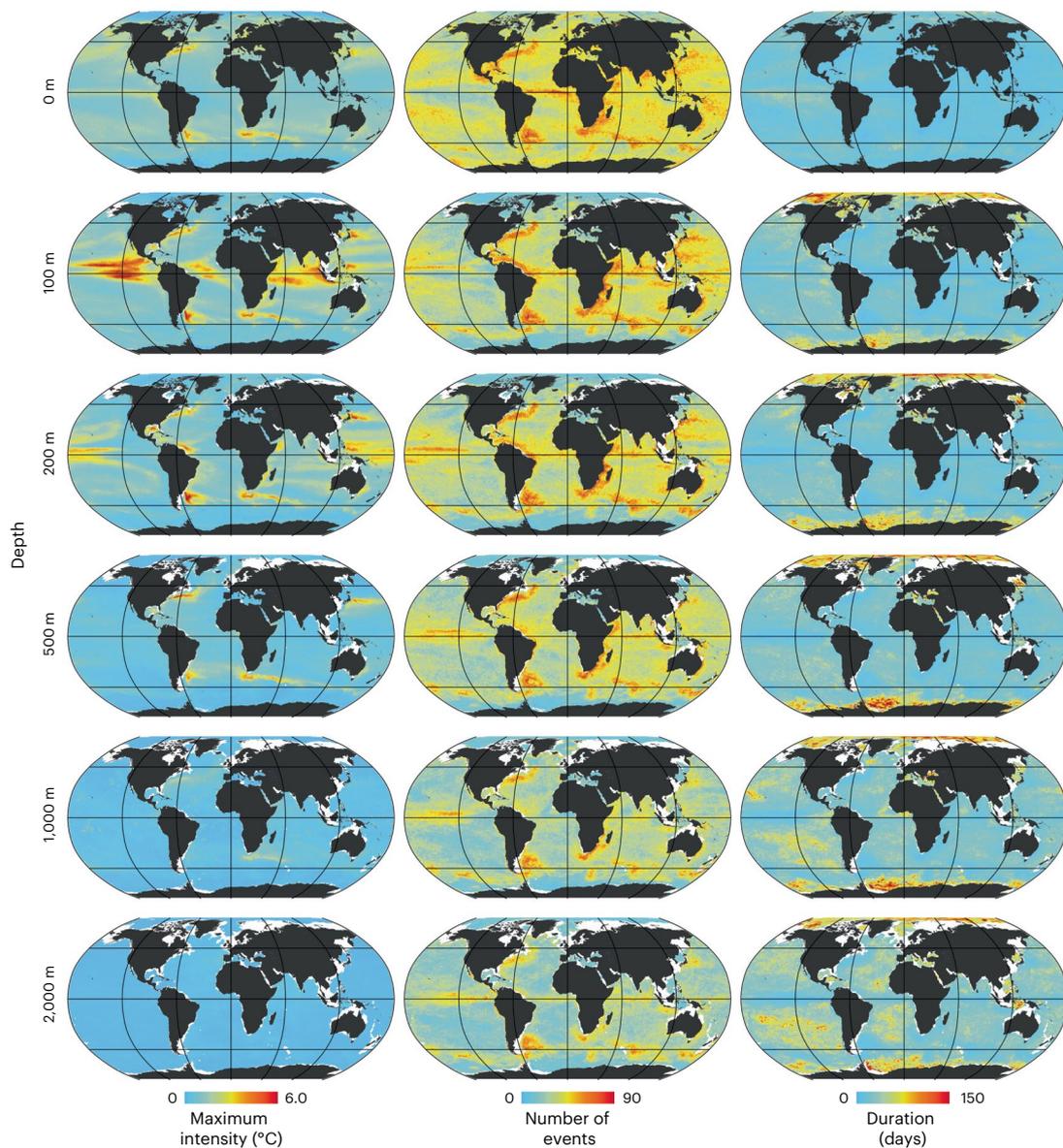
Fig. 2 | Spatial distribution of MHW metrics with depth for the period 1993–2019. Global maps depicting MHW maximum intensity (left column), occurrence (number of events from 1993 to 2019; middle column) and average duration (right column). White map areas have no corresponding data because the ocean floor does not reach these depths. Maps are presented in Robinson projection with the main graticules depicted. Scales have been adapted to improve visibility; full ranges can be found in Supplementary Table 3.

Discussion

Using state-of-the-art reanalysis data, we show that globally subsurface MHWs are, on average, longer and more intense than surface events, with up to 22% of the subsurface ocean being in the highest biodiversity exposure category. Biodiversity impacts could be greater in the upper 250 m of the ocean, where MHW (cumulative) intensity was the highest. This can be particularly concerning at the warm range edge of species' distribution, where thermal tolerances are easily exceeded and more impacts have been recorded[6,7]. Thus, potential depth and distribution range shifts are likely in the upper 250 m as a response to acute warming, driving changes in global biodiversity patterns with consequent effects on marine communities and ecological interactions[28,29]. However, the large variability found in the regional patterns of MHWs highlights a complex picture of biodiversity exposure across depths and regions.

Our results are consistent with previous regional findings[10–18] and show that strong subsurface MHWs are conspicuous across the

global ocean, with varying characteristics that depend on the prevailing oceanographic conditions. Surface events often extended to a considerable depth, particularly in regions of boundary currents and oceanographic fronts (Fig. 4a,b), but subsurface MHWs still occurred without a surface signal, driven by distinct mechanisms (Fig. 4c–e). MHW duration increased with depth across the ocean, yet the most prolonged events were often estimated in the subsurface of polar regions (Fig. 2). Despite the acknowledged uncertainties of polar estimates (Methods), additional studies corroborate the trends in our findings. The long-lasting subsurface MHWs in the Arctic Ocean are in line with its borealization by Atlantic[30] and Pacific[31] warm subsurface water flows at ~150–900 m depth. Similar trends of subsurface warming have been reported across the Antarctic[32], including the Weddell Sea[33], where we estimated long-lasting subsurface MHWs.

The spatial variation in MHW characteristics is suggestive of distinct driving mechanisms for different MHW types: the
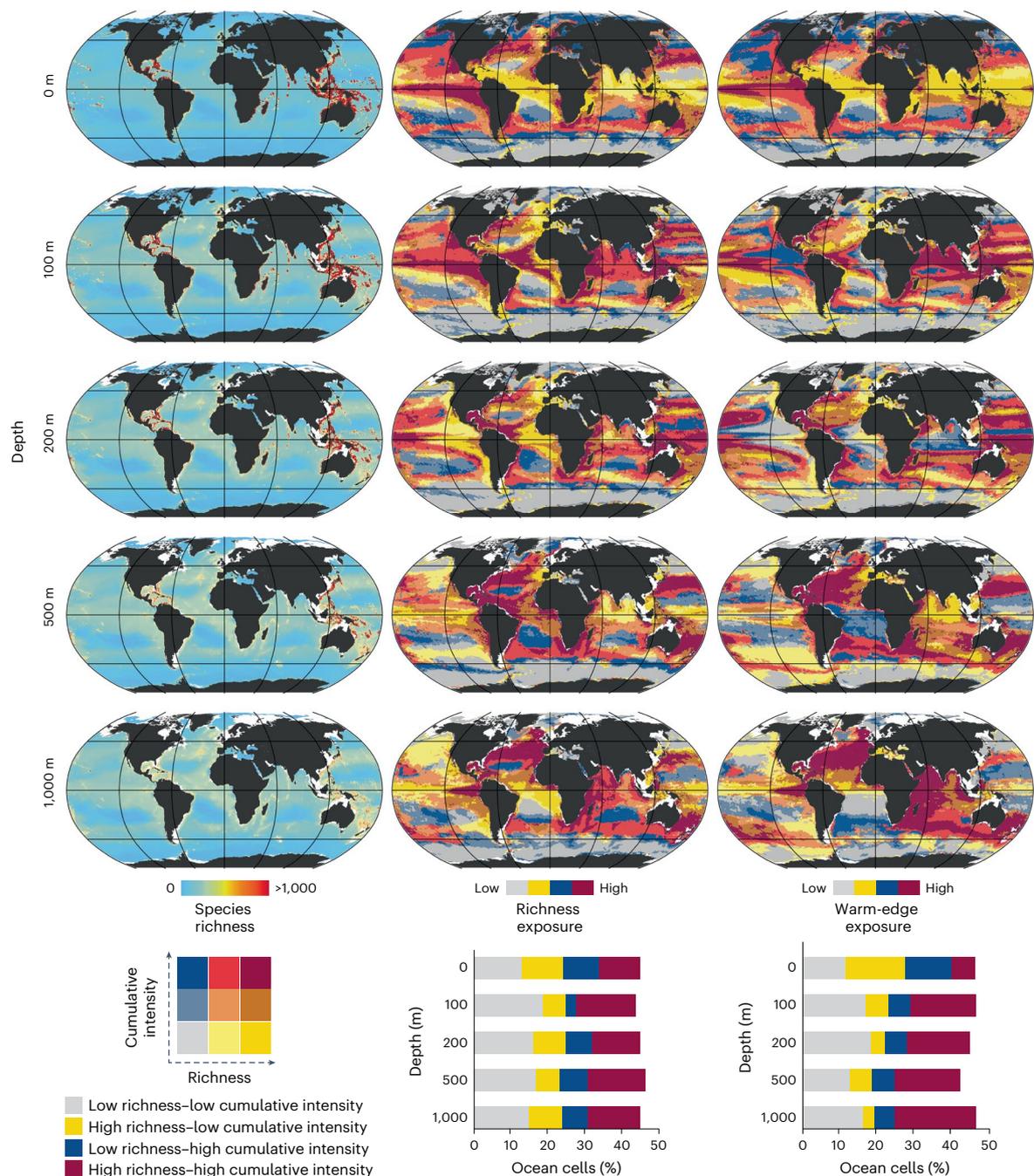
Fig. 3 | Spatial distribution of biodiversity exposure to MHWs with depth for the period 1993–2019. Global maps depicting species richness (left column), richness exposure (middle column) and warm-edge exposure to MHWs (right column). Cumulative intensity, species richness and warm-edge richness were divided into terciles. Exposure was defined as the overlap of tercile combinations between cumulative intensity and biodiversity metrics, forming nine exposure categories. The percentage of ocean cells for the four most extreme overlapping terciles is shown. White map areas have no corresponding data because the ocean floor does not reach these depths. Maps are presented in Robinson projection with the main graticules depicted.

surface-confined; those that are intensified in the subsurface or that do not have a surface expression; and those extending below the surface mixed layer (Fig. 4). Events confined to the mixed layer (for example, Fig. 4c and Supplementary Fig. 9c) are probably generated by surface drivers, such as surface currents[9,34,35] or anomalies in air–sea heat fluxes[34,35]. Yet, their depth extension may depend on the stratification of the water column (Supplementary Fig. 9c), with weak stratification linked to deeper warming[11,13,14,16,17]. Changes in seasonal timing, such as the beginning of monsoon season, can influence the background variability of the ocean (for example, salinity and

thermocline depth), thereby affecting the probability of subsurface MHW emergence, without a surface signal (for example, Fig. 4d)[10–17]. Specifically, changes in wind patterns can prevent MHW emergence through upwelling[36] or promote it through Ekman downwelling, driving subsurface MHWs below the mixed layer (Supplementary Fig. 9c,d), where warming is insulated from surface processes and therefore can last longer[10–12,14–17]. Rossby and equatorial Kelvin waves can also drive changes in the climate and circulation conditions, influencing the emergence of subsurface MHWs around the thermocline[17,37]. At boundary currents and fronts (Fig. 4a,b), MHWs can extend hundreds
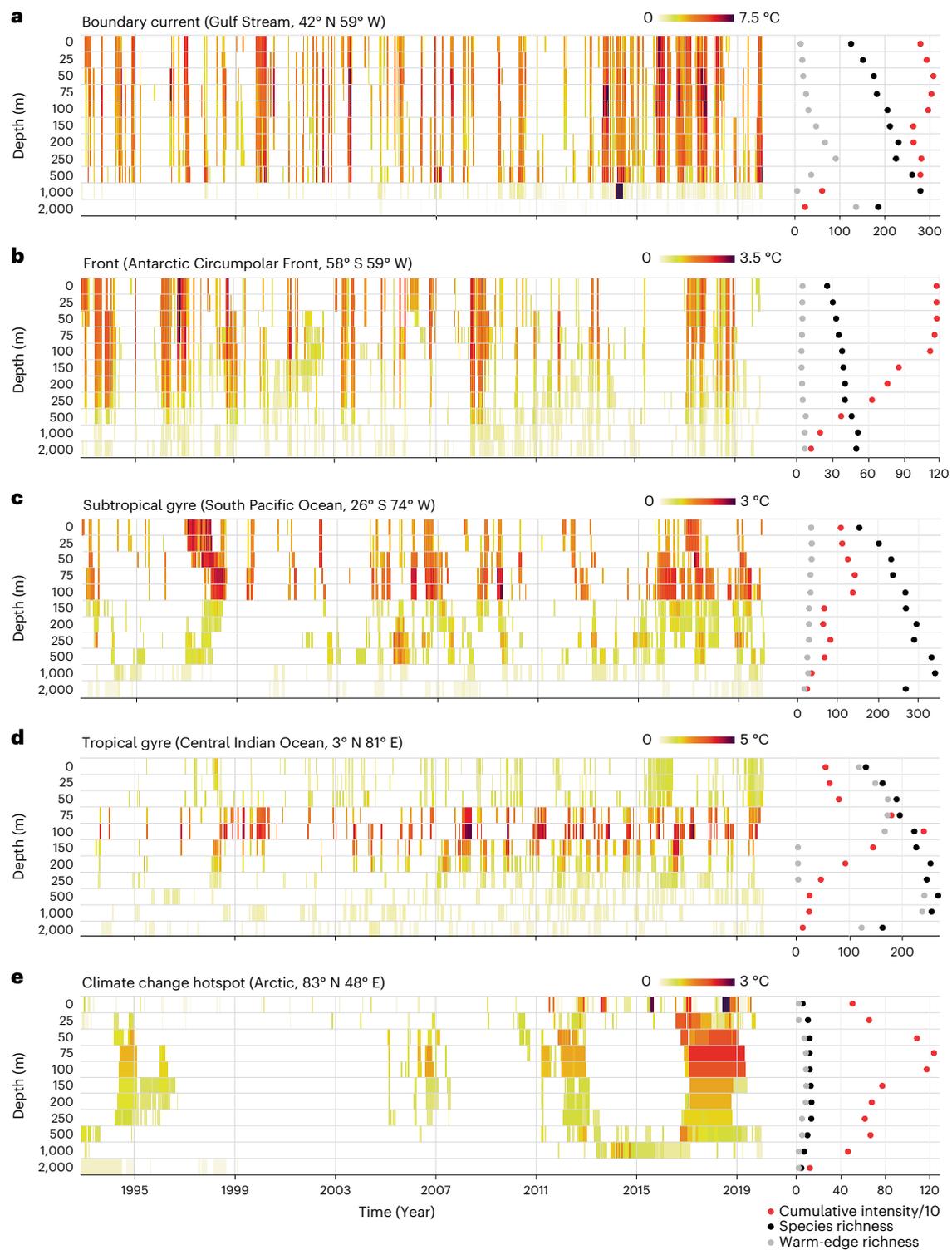
Fig. 4 | Local MHW and biodiversity patterns in selected regions of distinct oceanographic or climatic conditions. a–e, Time–depth maximum MHW intensity, cumulative intensity, species and warm-edge richness for boundary current (**a**), oceanographic front (**b**), subtropical (**c**) and tropical gyre (**d**), and Arctic Ocean (**e**). Depth levels and temperature scales are not to scale. Regional characteristics were estimated from a 2° × 2° resolution cell. The geographic location of each offshore region and additional analyses of replicate regions are shown in Extended Data Figs. 1 and 2.

of metres into the water column, well below the thermocline depth (Supplementary Fig. 9a,b), driven by anomalous current circulation[11,12,14,15,17,18], related to variations in their location, strength and heat content. Distinguishing the mechanisms driving each MHW event is challenging due to limited large-scale, long-term oceanographic and atmospheric data, as multiple, complex drivers can interact, favouring or preventing MHW emergence. Therefore, systematic monitoring of the global ocean across depths is necessary to enable a better understanding of subsurface MHW drivers and potential changes related to future climate change.

MHWs have caused abrupt ecosystem changes across the globe, triggering diverse ecophysiological responses of marine organisms[38–40]. Most responses have been reported from shallow coastal regions (<40 m[41]); however, we show high MHW (cumulative) intensities in the upper 250 m, translated into increased biodiversity exposure at depths, depending on the oceanographic conditions (for example, at 50–100 m in tropical gyres and 250–500 m in boundary currents). Coastal ecosystems, being readily accessible, are more frequently monitored and biodiversity responses of deeper ecosystems could be overlooked. Indeed, deep surveys have reported MHW impacts extending to mesopelagic reefs, down to 100 m depth[42–44]. MHW impacts can be particularly detrimental on warm range edge populations of sessile species[6,7], whose individuals cannot move to cooler waters. Characteristic examples include the coral bleaching in the Great Barrier Reef[45] and the extensive kelp forest losses in southern Australia and the northeastern Pacific[46,47]. In regions where multiple species have their warm range edges (that is, high warm-edge exposure), such as southwestern Australia and the coast of Alaska (Fig. 3), MHW effects can be magnified into entire community shifts, lasting for years after the events[38,39]. As MHWs become more frequent and intense under long-term warming[4], species depth ranges are expected to deepen[48] and may become vertically compressed[49], as already reported for cold-water species in the Mediterranean Sea[28]. However, where strong internal temperature variability prevails, such as in current fronts such as the Gulf Stream or at thermoclines like those of tropical gyres (Fig. 4a,d), populations may have adapted their physiological responses to local temperature conditions[50–53]. But despite species' plasticity, ecosystems can still suffer abrupt changes, especially when MHWs are frequent[54,55], prolonged[38] and coupled with additional disturbances[56,57].

Deeper than 250 m, MHWs are, on average, half as intense as at the surface (<1 °C). Empirical evidence of ecophysiological responses to thermal stress is limited for these ecosystems, but available reports show temperature changes of only 0.1–0.4 °C affecting species richness and community structure of nematodes at 1,500 m depth[58], and peracarid crustaceans at depths of 600–2,300 m[59]. This suggests that deep-sea biodiversity could be sensitive to small temperature changes. Despite the low intensities, MHWs in the deep ocean may still have implications for biodiversity, especially if coupled with declines in oxygen concentration, pH and organic material fluxes[60,61]. For example, despite the decrease in MHW cumulative intensity below 500 m depth, this depth coincides with oxygen minimum zones for vast regions of the ocean[61], therefore even a weak MHW could act synergistically on the response of the ecosystems. However, empirical evidence is needed to verify this hypothesis.

While most studies reporting the impact of extreme ocean temperatures on biodiversity are based on surface events, the high exposure found down to 250 m depth suggests that subsurface biodiversity is also at considerable risk. Previous work has shown that the main driver behind the increase in intensity and frequency of MHWs is ocean warming[5]. While ocean warming could be more near the surface, warming does persist in the deep ocean and is projected to increase in the future[62]. As such, future MHWs will probably become more frequent and intense across all depths, further exposing biodiversity to their effects. This might shift species' depth distributions, particularly in the upper to 250 m of the ocean, potentially changing global biodiversity patterns, with consequent effects on ecological interactions and ecosystem processes. However, these shifts may be hindered by low oxygen zones or the lack of species' physiological adaptations to the conditions of the deeper ocean[63]. Baseline empirical evidence and time-series analyses of deep-sea communities under MHWs are needed to acknowledge their responses to warming and increased MHWs, as those may be going unnoticed.

Online content

Any methods, additional references, Nature Portfolio reporting summaries, source data, extended data, supplementary information, acknowledgements, peer review information; details of author contributions and competing interests; and statements of data and code availability are available at https://doi.org/10.1038/s41558-023-01790-6.

References

1. Frölicher, T. L., Fischer, E. M. & Gruber, N. Marine heatwaves under global warming. *Nature* **560**, 360–364 (2018).
2. Oliver, E. C. J. et al. Longer and more frequent marine heatwaves over the past century. *Nat. Commun.* **9**, 1324 (2018).
3. Tanaka, K. R. & van Houtan, K. S. The recent normalization of historical marine heat extremes. *PLOS Clim.* **1**, e0000007 (2022).
4. Oliver, E. C. J. et al. Projected marine heatwaves in the 21st century and the potential for ecological impact. *Front. Mar. Sci.* **6**, 734 (2019).
5. Oliver, E. C. J. Mean warming not variability drives marine heatwave trends. *Clim. Dyn.* **53**, 1653–1659 (2019).
6. Smale, D. A. et al. Marine heatwaves threaten global biodiversity and the provision of ecosystem services. *Nat. Clim. Change* **9**, 306–312 (2019).
7. Smith, K. E. et al. Biological impacts of marine heatwaves. *Annu. Rev. Mar. Sci.* **15**, 119–145 (2023).
8. Smith, K. E. et al. Socioeconomic impacts of marine heatwaves: global issues and opportunities. *Science* **374**, eabj3593 (2021).
9. Oliver, E. C. J. et al. Marine heatwaves. *Annu. Rev. Mar. Sci.* **13**, 313–342 (2021).
10. Benthuysen, J. A., Oliver, E. C. J., Feng, M. & Marshall, A. G. Extreme marine warming across tropical Australia during austral summer 2015–2016. *J. Geophys. Res. Oceans* **123**, 1301–1326 (2018).
11. Elzahaby, Y. & Schaeffer, A. Observational insight into the subsurface anomalies of marine heatwaves. *Front Mar. Sci.* **6**, 745 (2019).
12. Elzahaby, Y., Schaeffer, A., Roughan, M. & Delaux, S. Oceanic circulation drives the deepest and longest marine heatwaves in the East Australian Current system. *Geophys. Res. Lett.* **48**, e2021GL094785 (2021).
13. Scannell, H. A., Johnson, G. C., Thompson, L., Lyman, J. M. & Riser, S. C. Subsurface evolution and persistence of marine heatwaves in the northeast Pacific. *Geophys. Res. Lett.* **47**, e2020GL090548 (2020).
14. Ryan, S. et al. Depth structure of Ningaloo Niño/Niña events and associated drivers. *J. Clim.* **34**, 1767–1788 (2021).
15. Oliver, E. C. J. et al. Marine heatwaves off eastern Tasmania: trends, interannual variability, and predictability. *Prog. Oceanogr.* **161**, 116–130 (2018).
16. Schaeffer, A. & Roughan, M. Subsurface intensification of marine heatwaves off southeastern Australia: the role of stratification and local winds. *Geophys. Res. Lett.* **44**, 5025–5033 (2017).
17. Hu, S. et al. Observed strong subsurface marine heatwaves in the tropical western Pacific Ocean. *Environ. Res. Lett.* **16**, 104024 (2021).
18. Großelindemann, H., Ryan, S., Ummenhofer, C. C., Martin, T. & Biastoch, A. Marine heatwaves and their depth structures on the northeast U.S. continental shelf. *Front. Clim.* **4**, 857937 (2022).
19. Jackson, J. M., Johnson, G. C., Dosser, H. V. & Ross, T. Warming from recent marine heatwave lingers in deep British Columbia fjord. *Geophys. Res. Lett.* **45**, 9757–9764 (2018).
20. Holbrook, N. J. et al. Keeping pace with marine heatwaves. *Nat. Rev. Earth Environ.* **1**, 482–493 (2020).
21. *Global Ocean Physics Reanalysis* (EU Copernicus Marine Service Information (CMEMS) and Marine Data Store (MDS), accessed 13 May 2021); https://doi.org/10.48670/moi-00021
22. Brito-Morales, I. et al. Climate velocity reveals increasing exposure of deep-ocean biodiversity to future warming. *Nat. Clim. Change* **10**, 576–581 (2020).

23. Kaschner, K. et al. *AquaMaps: Predicted Range Maps for Aquatic Species* (2019). Retrieved from https://www.aquamaps.org

24. Jacox, M. G. et al. Impacts of the 2015–2016 El Niño on the California Current system: early assessment and comparison to past events. *Geophys. Res. Lett.* **43**, 7072–7080 (2016).

25. Hobday, A. J. et al. A hierarchical approach to defining marine heatwaves. *Prog. Oceanogr.* **141**, 227–238 (2016).

26. Holte, J., Talley, L. D., Gilson, J. & Roemmich, D. An Argo mixed layer climatology and database. *Geophys. Res. Lett.* **44**, 5618–5626 (2017).

27. Imawaki, S. et al. in *Observing the Oceans in the 21st Century* (eds Koblinsky, C. & Smith, N.) 285–306 (Godae Project Office, Bureau of Meteorology, 2001).

28. Chaikin, S., Dubiner, S. & Belmaker, J. Cold-water species deepen to escape warm water temperatures. *Glob. Ecol. Biogeogr.* **31**, 75–88 (2022).

29. Cartes, J. E. et al. Changes in deep-sea fish and crustacean communities at 1000–2200m in the western Mediterranean after 25 years: relation to hydro-climatic conditions. *J. Mar. Syst.* **143**, 138–153 (2015).

30. Polyakov, I. V. et al. Greater role for Atlantic inflows on sea-ice loss in the Eurasian basin of the Arctic Ocean. *Science* **356**, 285–291 (2017).

31. Woodgate, R. A. Increases in the Pacific inflow to the Arctic from 1990 to 2015, and insights into seasonal trends and driving mechanisms from year-round Bering Strait mooring data. *Prog. Oceanogr.* **160**, 124–154 (2018).

32. Schmidtko, S., Heywood, K. J., Thompson, A. F. & Aoki, S. Multidecadal warming of Antarctic waters. *Science* **346**, 1227–1231 (2014).

33. Strass, V. H. et al. Multidecadal warming and density loss in the deep Weddell Sea, Antarctica. *J. Clim.* **33**, 9863–9881 (2020).

34. Holbrook, N. J. et al. A global assessment of marine heatwaves and their drivers. *Nat. Commun.* **10**, 2624 (2019).

35. sen Gupta, A. et al. Drivers and impacts of the most extreme marine heatwaves events. *Sci. Rep.* **10**, 19359 (2020).

36. Varela, R., Rodríguez-Díaz, L., de Castro, M. & Gómez-Gesteira, M. Influence of eastern upwelling systems on marine heatwaves occurrence. *Glob. Planet. Change* **196**, 103379 (2021).

37. Pinault, J. L. A review of the role of the oceanic Rossby waves in climate variability. *J. Mar. Sci. Eng.* **10**, 493 (2022).

38. Suryan, R. M. et al. Ecosystem response persists after a prolonged marine heatwave. *Sci. Rep.* **11**, 6235 (2021).

39. Wernberg, T. et al. Climate-driven regime shift of a temperate marine ecosystem. *Science* **353**, 169–172 (2016).

40. Straub, S. C. et al. Resistance, extinction, and everything in between – the diverse responses of seaweeds to marine heatwaves. *Front. Mar. Sci.* **6**, 763 (2019).

41. Garrabou, J. et al. Collaborative database to track mass mortality events in the Mediterranean Sea. *Front. Mar. Sci.* **6**, 707 (2019).

42. Haguenauer, A. et al. Deep heat: a comparison of water temperature, anemone bleaching, anemonefish density and reproduction between shallow and mesophotic reefs. *Fishes* **6**, 37 (2021).

43. Bavestrello, G. et al. The red coral populations of the gulfs of Naples and Salerno: human impact and deep mass mortalities. *Ital. J. Zool.* **81**, 552–563 (2014).

44. Perkins, N. R. et al. Bleaching in sponges on temperate mesophotic reefs observed following marine heatwave events. *Clim. Change Ecol.* **3**, 100046 (2022).

45. Hughes, T. P. et al. Global warming and recurrent mass bleaching of corals. *Nature* **543**, 373–377 (2017).

46. Arafeh-Dalmau, N. et al. Extreme marine heatwaves alter kelp forest community near its equatorward distribution limit. *Front. Mar. Sci.* **6**, 499 (2019).

47. Wernberg, T. in *Ecosystem Collapse and Climate* Change (eds Canadell, J. G. & Jackson, R. B.) 325–343 (Springer Nature, 2021).

48. Santana-Falcón, Y. & Séférian, R. Climate change impacts the vertical structure of marine ecosystem thermal ranges. *Nat. Clim. Change* **12**, 935–942 (2022).

49. Jorda, G. et al. Ocean warming compresses the three-dimensional habitat of marine life. *Nat. Ecol. Evol.* **4**, 109–114 (2020).

50. Gouvêa, L. P. et al. Phenotypic plasticity in sargassum forests may not counteract projected biomass losses along a broad latitudinal gradient. *Ecosystems* **26**, 29–41 (2022).

51. Schubert, N., Santos, R. & Silva, J. Living in a fluctuating environment increases tolerance to marine heatwaves in the free-living coralline alga *Phymatolithon lusitanicum*. *Front. Mar. Sci.* **8**, 791422 (2021).

52. Coleman, M. A. & Wernberg, T. The silver lining of extreme events. *Trends Ecol. Evol.* **35**, 1065–1067 (2020).

53. Pershing, A. J. et al. Evidence for adaptation from the 2016 marine heatwave in the northwest Atlantic Ocean. *Oceanography* **31**, 152–161 (2018).

54. Seuront, L. et al. Decreased thermal tolerance under recurrent heat stress conditions explains summer mass mortality of the blue mussel *Mytilus edulis*. *Sci. Rep.* **9**, 17498 (2019).

55. Dalton, S. J. et al. Successive marine heatwaves cause disproportionate coral bleaching during a fast phase transition from El Niño to La Niña. *Sci. Total Environ.* **715**, 136951 (2020).

56. Rogers-Bennett, L. & Catton, C. A. Marine heat wave and multiple stressors tip bull kelp forest to sea urchin barrens. *Sci. Rep.* **9**, 15050 (2019).

57. Donovan, M. K. et al. Local conditions magnify coral loss after marine heatwaves. *Science* **372**, 977–980 (2021).

58. Danovaro, R., Dell'Anno, A. & Pusceddu, A. Biodiversity response to climate change in a warm deep sea. *Ecol. Lett.* **7**, 821–828 (2004).

59. Ashford, O. S. et al. Phylogenetic and functional evidence suggests that deep-ocean ecosystems are highly sensitive to environmental change and direct human disturbance. *Proc. R. Soc. B* **285**, 1–10 (2018).

60. Sweetman, A. K. et al. Major impacts of climate change on deep-sea benthic ecosystems. *Elem. Sci. Anth.* **5**, 4 (2017).

61. Shi, Z., Assis, J. & Costello, M. J. in *Imperiled: The Encyclopedia of Conservation* (eds DellaSala, D. A. & Goldstein, M. I.) 887–894 (Elsevier, 2022).

62. IPCC *Climate Change 2021: The Physical Science Basis* (eds Masson-Delmotte, V. et al.) (Cambridge Univ. Press, 2021).

63. Gerringer, M. E. et al. Habitat influences skeletal morphology and density in the snailfishes (family Liparidae). *Front. Zool.* **18**, 16 (2021).

Methods

Daily global temperature data with depth covering 1993–2019

MHW characteristics were estimated using daily temperature time series derived from the Global Ocean Physics Reanalysis (GLORYS12V1)[21] provided by the EU Copernicus Marine Service. This is an eddy-permitting (1/12°) ocean reanalysis based on the Nucleus for European Modelling of the Ocean ocean model. The model is forced by the global atmospheric reanalysis ERA-Interim (between 1993 and 2018) and its successor the ERA5 reanalysis subsequently, and assimilates satellite altimetry, sea surface temperature and sea-ice data as well as in-situ temperature and salinity profiles from the Coriolis Ocean database ReAnalysis (CORA)[64], which has global coverage and includes Argo data (Supplementary Fig. 1). Temperature data are available at 50 depth levels covering the period 1993–2019.

The ability of the GLORYS12V1 reanalysis to capture ocean processes has been previously verified against in-situ observations and alternative models at local[65–67] and global[68] scales. However, some regional limitations exist. Specifically, the GLORYS12V1 shows a higher than observed warming trend[68] and temperature biases (up to 1.2 °C) occurring in the 50–100 m depth in the Atlantic and 50–200 m depth in the Indian Ocean[69]. Because MHW estimates depend on temperature variability and not on mean temperature[25], we assessed the temporal variation of GLORYS12V1 against daily in-situ temperature datasets. Cross-validation was performed between daily in-situ records, at the available locations (geographical position, depth and date), and the nearest cell from the GLORYS12V1 reanalysis (as in refs. [69],[70]). The paired relationships were statistically compared based on the mean absolute error (MAE) of temperature, the mean absolute error of temperature variance from the mean (MAEvar) and Pearson's correlation. The cross-validation scheme was based on three different in-situ datasets (Supplementary Fig. 2): (1) the 'polar moorings' time series dataset (independent data that have not been assimilated in the reanalysis model) consisted of 47 moorings from 13 sources (Supplementary Table 1), resulting in 1.09 million daily temperature records at different depths; (2) the 'NOAA' time series dataset (assimilated in the reanalysis model) consisted of 70 TAO/TRITON moorings in the tropical Pacific and 20 PIRATA moorings in the Atlantic from the NOAA Pacific Marine Environmental Laboratory[71], covering the period from 1993 to 2019, and resulting in 7.6 million daily temperature records at different depths; and (3) the Global Ocean Data Analysis Project (GLODAPv2.1) dataset[72] (independent data that have not been assimilated in the reanalysis model), derived by quality-controlled temperature observations from cruises across the global ocean, resulting in 680,777 records at different depths. Because the GLODAPv2.1 dataset does not provide temperature in time series, only spatial differences in temperature were assessed and not temporal variability.

Cross-correlations of the GLORYS12V1 against the polar moorings resulted in a MAE of 0.075 °C, MAEvar of 1.4×10^{-15} °C and a mean correlation across depths of 0.842 (Supplementary Table 2). The lowest correlations were estimated at 150–500 m depth, ranging from 0.459 to 0.601 and the largest MAE of 0.426 °C between 0 and 25 m depth (Supplementary Table 2). Cross-correlations against the NOAA moorings resulted in a MAE of 0.101 °C, MAEvar of 1.8×10^{-15} °C and a mean correlation for all depths of 0.991 (Supplementary Table 2). The lowest correlation (0.858) was estimated at 500–1,000 m depth and the larger MAE of 1.2 °C between 200 and 250 m depth. Cross-correlations against the GLODAPv2.1 dataset resulted in a MAE of 0.049 °C and a mean correlation of 0.996 (Supplementary Table 2). The lowest correlation (0.983) was estimated at 500–1,000 m depth and the larger MAE of 0.23 °C between 200 and 250 m depth. Examples of correlation plots of temperature variability between the GLORYS12V1 and the in-situ time series are presented in Supplementary Figs. 3 and 4, and all plots are available on Figshare (https://doi.org/10.6084/m9.figshare.19174985). Also, scatterplots of the temperature correlation between the GLORYS12V1 and each of the three in-situ datasets are presented in Supplementary Figs. 5–7. Lastly, the spatial distribution of temperature errors (Supplementary Fig. 8)

for each depth was mapped onto a 2.5° grid by determining the average difference between the GLORYS12V1 and all three in-situ datasets[70]. Analyses revealed a spatial distribution of errors being larger between 50 and 250 m depth, reaching regionally up to 6 °C (Supplementary Fig. 8). However, temperature differences were mostly restricted to regions of the northwestern (in the extension of the Gulf Stream) and central Atlantic Ocean (Supplementary Fig. 8). Despite the regional temperature errors, correlations in temperature variability between the reanalysis and in-situ datasets were still high, therefore not affecting the MHW estimates that depend on temperature variability and not on mean temperature.

Overall, we show that the GLORYS12V1 captures well temperature variability and can be used to estimate MHWs across the global ocean, despite the existing regional differences against the in-situ datasets. Yet, it is important to acknowledge that the reanalysis may still carry biases that influence the prediction of extreme events, especially in regions/depths where lower correlations were found. Specifically in polar regions, where the lowest correlations between the reanalysis and in-situ datasets were found, MHW estimates have higher uncertainty, due to the reduced number of in-situ data feeding the model.

Spatial and depth resolution of global MHW estimates

The GLORYS12V1 dataset were re-gridded onto an equal-area 60-km-resolution hexagon grid (approx. 0.5° resolution) using Uber's standardized hexagonal hierarchical spatial data gridding system[73]. Mean daily temperatures were retrieved for each hexagon to produce distinct baseline climatologies for the identification of MHW events at 11 depths: 0, 25, 50, 75, 100, 150, 200, 250, 500, 1,000 and 2,000 m. Uber's hexagonal framework was chosen due to its equal-area projection and optimal indexing algorithm, which allows fast data aggregation over its hierarchical resolutions[73].

MHW analyses and characteristics with depth

MHW events were identified following ref. [25], which defines a MHW as a discrete prolonged anomalously warm water event of at least 5-day duration, during which daily temperatures exceeded the 90th percentile threshold of the historical baseline climatology (in our case, 27 years, from 1993 to 2019). Events less than 3 days apart were considered a single event. The historical baseline climatology for a given day was calculated using an 11-day window centred on that date across all years of the climatology period, and an additional 31-day moving average was applied to smooth the climatology[25]. A daily varying threshold was preferred to an absolute fixed value, as it allowed the identification of MHW events throughout the year, rather than during the warmest seasons only. Each MHW event was characterized by a set of metrics[25], namely, the duration (days), maximum intensity (°C), cumulative intensity (°C days) and the absolute temperature (°C) of the ocean at the peak of maximum intensity. Metrics were estimated independently for each depth. Regional (hexagon) estimates were calculated as the average of each metric for the years 1993–2019.

Regional MHW occurrence was calculated as the total number of events from 1993 to 2019 in each hexagon. Global estimates per depth were calculated as the average of all hexagons for each depth. Regional time–depth MHW and biodiversity (see below) metrics (that is, MHW maximum intensity, cumulative intensity, temperature profiles, species richness and warm-edge richness) were calculated as the daily average of hexagons at a 2° × 2° resolution for each depth.

To explore potential temporal synchrony between the warming of the surface and subsurface layers, Pearson's correlation coefficients for temperature anomalies were determined and P values were estimated as a measure of statistical significance ($P < 0.05$) using the package 'synchrony'[74] which accounts for temporal autocorrelation.

Biodiversity data

We used species richness as an indicator of biodiversity. Richness was estimated from 25,078 modelled marine species ranges available in AquaMaps[23], including fishes, invertebrates, mammals, algae

and seagrasses. AquaMaps produces standardized species distribution maps using a probability of occurrence threshold (0–1) resulting from environmental niche models at 0.5° resolution. Here, we used a minimum threshold of 0.5 probability of occurrence to define species ranges[22,75]. Considering the depth preferences of each species provided by the AquaMaps database, we categorized their distributions on the depth layers for which MHWs were estimated. Species richness was estimated as the number of species with distribution ranges within each hexagon grid (approx. 0.5° resolution). Because populations at the warm range edge of their distribution are more likely to exceed their thermal tolerance when exposed to MHWs[6], we inferred temperature-sensitive populations for each species by dividing their distribution into terciles, corresponding to the cold, central and warm distribution range edge[6], based on the average temperature from 1993 to 2019 (derived from the same daily data used to estimate MHWs). Warm-edge richness was determined as the number of species at their warm range edge within each hexagon. Estimates of species richness, warm-edge richness and cumulative intensity at a given depth were divided into terciles, corresponding to low, medium and high values[22], and hexagons were reclassified accordingly. We estimated potential richness/warm-edge exposure as the overlap of MHW cumulative intensity (as a measure of cumulative heat stress on biodiversity[76,77]) and species richness/warm-edge richness per hexagon. Nine exposure categories were defined as the overlap of tercile combinations between cumulative intensity and biodiversity metrics. The highest exposure was considered in cells where high cumulative intensity overlapped high species richness/warm-edge richness. In contrast, the lowest exposure was considered in cells where low cumulative intensity overlapped high species richness/ warm-edge richness.

All analyses were conducted in R[78] and the code is openly available on Figshare[79]. MHWs were estimated using the package 'RmarineHeatWaves' and thermocline depth was estimated using the function 'thermo.depth' of the 'rLAkeAnalyzer'. Individual global maps depicting MHW and biodiversity metrics can be found on Figshare (https://doi.org/10.6084/m9.figshare.19174985).

Reporting summary

Further information on research design is available in the Nature Portfolio Reporting Summary linked to this article.

Data availability
Daily temperature reanalysis data (GLORYS12V1) are openly provided by the EU Copernicus Marine Service (https://doi.org/10.48670/moi-00021). The biodiversity dataset is openly available from AquaMaps at https://www.aquamaps.org. The datasets used for the validation of the GLORYS12V1 reanalysis are: (1) the NOAA dataset (https://doi.org/10.5270/OceanObs09.cwp.61), available for download at https://www.pmel.noaa.gov/tao/drupal/disdel/; (2) the GLODAPv2 dataset (https://doi.org/10.5194/essd-13-5565-2021) available for download at https://www.glodap.info/index.php/merged-and-adjusted-data-product-v22021/; and (3) the 'polar moorings' dataset, for which sources and detailed information can be found in Supplementary Table 1.

Code availability
R code for data collection and MHW analyses is openly available on Figshare (https://doi.org/10.6084/m9.figshare.19174985).

References

64. Szekely, T., Gourrion, J., Pouliquen, S. & Reverdin, G. *CORA, Coriolis Ocean Dataset for Reanalysis* (SEANOE, 2023); https://doi.org/10.17882/46219
65. Verezemskaya, P. et al. Assessing eddying (1/12°) ocean reanalysis GLORYS12 using the 14-yr instrumental record from 59.5° N section in the Atlantic. *J. Geophys. Res. Oceans* **126**, e2020JC016317 (2021).
66. Artana, C. et al. The Malvinas Current at the confluence with the Brazil Current: inferences from 25 years of Mercator Ocean reanalysis. *J. Geophys. Res. Oceans* **124**, 7178–7200 (2019).
67. Poli, L. et al. Anatomy of subinertial waves along the Patagonian shelf break in a 1/12° global operational model. *J. Geophys. Res. Oceans* **125**, e2020JC016549 (2020).
68. Lellouche, J.-M. et al. The Copernicus global 1/12° oceanic and sea ice GLORYS12 reanalysis. *Front. Earth Sci.* **9**, 698876 (2021).
69. Drévillon, M. et al. *Quality Information Document for Global Ocean Reanalysis Products: GLOBAL_REANALYSIS_PHY_001_030* (EU Copernicus Marine Service, 2021); https://catalogue.marine.copernicus.eu/documents/QUID/CMEMS-GLO-QUID-001-030.pdf
70. Assis, J. et al. Bio-ORACLE v2.0: extending marine data layers for bioclimatic modelling. *Glob. Ecol. Biogeogr.* **27**, 277–284 (2018).
71. McPhaden, M. J. et al. The global tropical moored buoy array. In *Proc. OceanObs'09: Sustained Ocean Observations and Information for Society* 668–682 (European Space Agency, 2010); https://www.aoml.noaa.gov/phod/docs/McPhaden_TheGlobalTropical.pdf
72. Olsen, A. et al. The Global Ocean Data Analysis Project version 2 (GLODAPv2) – an internally consistent data product for the world ocean. *Earth Syst. Sci. Data* **8**, 297–323 (2016).
73. Bondaruk, B., Roberts, S. A. & Robertson, C. Assessing the state of the art in discrete global grid systems: OGC criteria and present functionality. *Geomatica* **74**, 9–30 (2020).
74. Gouhier, T. C. & Guichard, F. Synchrony: quantifying variability in space and time. *Methods Ecol. Evol.* **5**, 524–533 (2014).
75. Klein, C. J. et al. Shortfalls in the global protected area network at representing marine biodiversity. *Sci. Rep.* **5**, 17539 (2015).
76. Laufkötter, C., Zscheischler, J. & Frölicher, T. L. High-impact marine heatwaves attributable to human-induced global warming. *Science* **369**, 1621–1625 (2020).
77. Wyatt, A. S. J. et al. Hidden heatwaves and severe coral bleaching linked to mesoscale eddies and thermocline dynamics. *Nat. Commun.* **14**, 25 (2023).
78. R Core Team *R: A Language and Environment for Statistical Computing* (R Foundation for Statistical Computing, 2021); https://www.R-project.org
79. Fragkopoulou, E. et al. Marine biodiversity exposed to prolonged and intense subsurface heatwaves. *Figshare* https://doi.org/10.6084/m9.figshare.19174985 (2023).

Acknowledgements

Author contributions

E.F., J.A. and O.D.C. conceived the study. E.F. and J.A. conducted the analyses. E.F. led the writing with the support of all authors. All authors revised the final draft and approved the submitted paper.

Extended Data Fig. 1 | See next page for caption.

Extended Data Fig. 1 | Local marine heatwave (MHW) and biodiversity patterns in selected regions of distinct oceanographic or climatic conditions. Global map depicting the geographic location of (**a**) boundary current, (**b**) oceanographic front, (**c**) subtropical and (**d**) tropical gyre, and (**e**) Arctic Ocean. Time-depth maximum MHW intensity, cumulative intensity, species and warm-edge richness are shown for regions of boundary current and oceanographic front (remaining regions are shown in Extended Data Fig. 2). Depth levels and temperature scales are not to scale. Regional characteristics were estimated from a 2 by 2-degree resolution cell. The global map features MHW cumulative intensity at the surface.
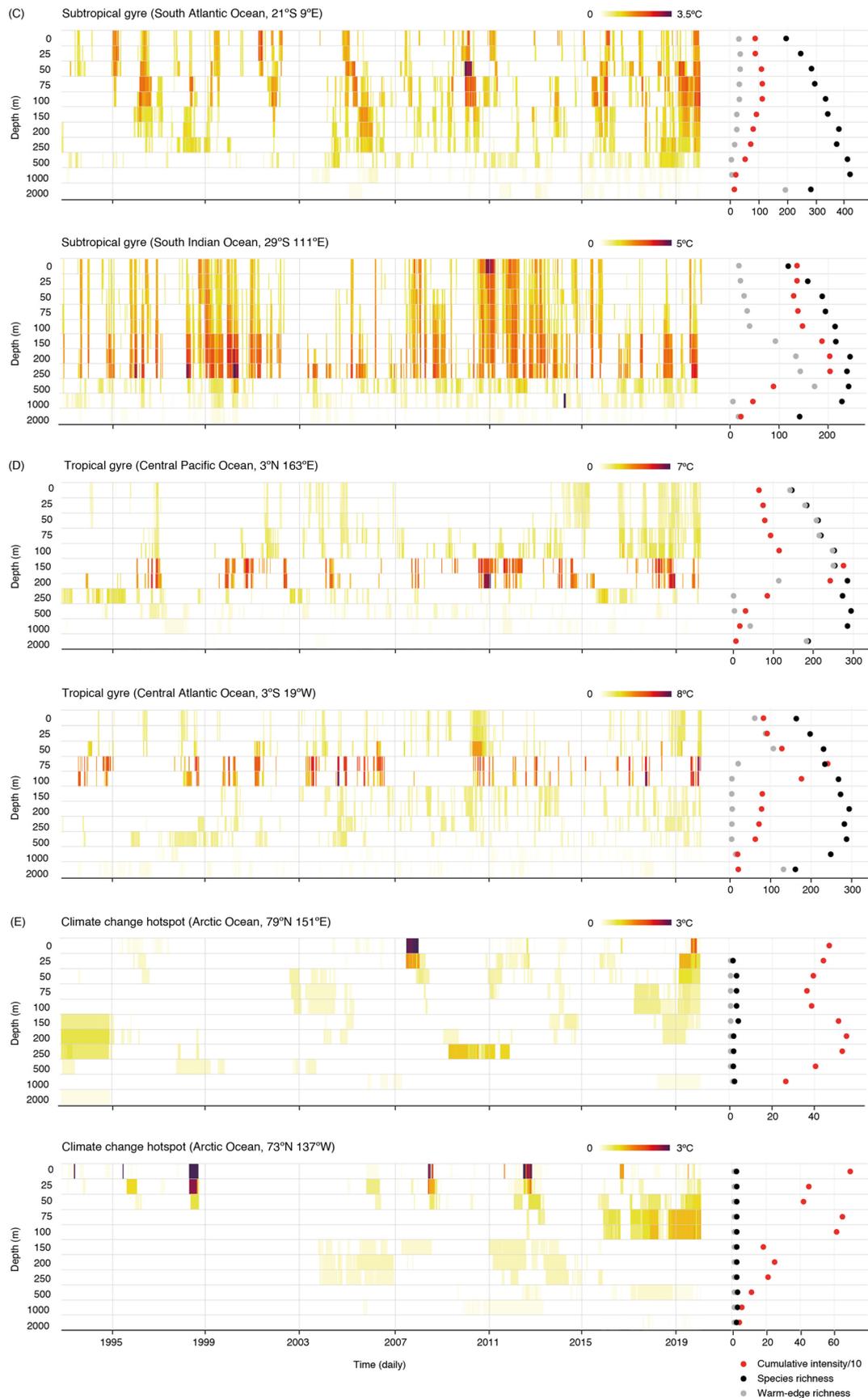
Extended Data Fig. 2 | Local marine heatwave (MHW) and biodiversity patterns in selected regions of distinct oceanographic or climatic conditions. (Continuous from Extended Data Fig. 1) Time-depth maximum MHW intensity, cumulative intensity, species and warm-edge richness for regions of **(C)** subtropical and **(D)** tropical gyre, and **(E)** Arctic Ocean. Depth levels and temperature scales are not to scale. Regional characteristics were estimated from a 2 by 2-degree resolution cell. The geographic location of each region is depicted in the global map of Extended Data Fig. 1.

nature research

Corresponding author(s): Eliza Fragkopoulou (eli_frag@hotmail.com); Jorge Assis (jorgefma@gmail.com)

Last updated by author(s): 2023/07/18

Reporting Summary

Nature Research wishes to improve the reproducibility of the work that we publish. This form provides structure for consistency and transparency in reporting. For further information on Nature Research policies, see our Editorial Policies and the Editorial Policy Checklist.

Statistics

For all statistical analyses, confirm that the following items are present in the figure legend, table legend, main text, or Methods section.

n/a	Confirmed	
☐	☒	The exact sample size (n) for each experimental group/condition, given as a discrete number and unit of measurement
☒	☐	A statement on whether measurements were taken from distinct samples or whether the same sample was measured repeatedly
☐	☒	The statistical test(s) used AND whether they are one- or two-sided *Only common tests should be described solely by name; describe more complex techniques in the Methods section.*
☐	☒	A description of all covariates tested
☒	☐	A description of any assumptions or corrections, such as tests of normality and adjustment for multiple comparisons
☐	☒	A full description of the statistical parameters including central tendency (e.g. means) or other basic estimates (e.g. regression coefficient) AND variation (e.g. standard deviation) or associated estimates of uncertainty (e.g. confidence intervals)
☐	☒	For null hypothesis testing, the test statistic (e.g. F, t, r) with confidence intervals, effect sizes, degrees of freedom and P value noted *Give P values as exact values whenever suitable.*
☒	☐	For Bayesian analysis, information on the choice of priors and Markov chain Monte Carlo settings
☒	☐	For hierarchical and complex designs, identification of the appropriate level for tests and full reporting of outcomes
☐	☒	Estimates of effect sizes (e.g. Cohen's d, Pearson's r), indicating how they were calculated

Our web collection on statistics for biologists contains articles on many of the points above.

Software and code

Policy information about availability of computer code

Data collection	Daily temperature reanalysis data (GLORYS12V1) collection was conducted in R statistical environment (version 4.1.3 2022). The biodiversity dataset and the in situ datasets for temperature validation were downloaded from online repositories (sources indicated in data availability statements).
Data analysis	All analysis were conducted in R statistical environment (version 4.1.3 2022). Packages "synchrony" (version 0.3.8), "RmarineHeatWaves" (version 0.17.0) and "rLAkeAnalyser" (version 1.11.4.1) were used in the analyses. R code is openly available on Figshare (https://doi.org/10.6084/m9.figshare.19174985).

For manuscripts utilizing custom algorithms or software that are central to the research but not yet described in published literature, software must be made available to editors and reviewers. We strongly encourage code deposition in a community repository (e.g. GitHub). See the Nature Research guidelines for submitting code & software for further information.

Data

Policy information about availability of data

All manuscripts must include a data availability statement. This statement should provide the following information, where applicable:

- Accession codes, unique identifiers, or web links for publicly available datasets
- A list of figures that have associated raw data
- A description of any restrictions on data availability

Daily temperature reanalysis data (GLORYS12V1) are openly provided by the E.U. Copernicus Marine Service (https://doi.org/10.48670/moi-00021). The biodiversity dataset is openly available from Aquamaps at https://www.aquamaps.org. The datasets used for the validation of the GLORYS12V1 reanalysis are: (1) the NOAA dataset (https://doi.org/10.5270/OceanObs09.cwp.61), available for download at: https://www.pmel.noaa.gov/tao/drupal/disdel/, and (2) the GLODAPv2 dataset

nature research | reporting summary

(https://doi.org/10.5194/essd-13-5565-2021) available for download at: https://www.glodap.info/index.php/merged-and-adjusted-data-product-v22021/. Sources and detailed information on the (3) "polar moorings" dataset can be found in Supplementary Material 1 Table 1.

Field-specific reporting

Please select the one below that is the best fit for your research. If you are not sure, read the appropriate sections before making your selection.

☐ Life sciences   ☐ Behavioural & social sciences   ☒ Ecological, evolutionary & environmental sciences

For a reference copy of the document with all sections, see nature.com/documents/nr-reporting-summary-flat.pdf

Ecological, evolutionary & environmental sciences study design

All studies must disclose on these points even when the disclosure is negative.

Study description	We estimate marine heatwaves (MHWs) in the global ocean from the surface to 2000 m depth and infer potential biodiversity exposure by overlapping species richness estimates with cumulative MHW intensity. MHWs were defined and metrics were estimated using the well-established approach of Hobday et al., 2016 (doi: 10.1016/j.pocean.2015.12.014).
Research sample	Openly available daily temperature reanalysis dataset at eleven depths (0, 25, 50, 75, 100, 150, 200, 250, 500, 1000, 2000 m) from the Copernicus Marine Service and biodiversity range maps for 25078 marine species from AquaMaps.
Sampling strategy	Openly available global datasets were retrieved from the above mentioned sources.
Data collection	Daily temperature reanalysis dataset was accessed through R statistical environment (code available at Figshare; https://doi.org/10.6084/m9.figshare.19174985). Biodiversity data were requested and accessed from AquaMaps at https://www.aquamaps.org.
Timing and spatial scale	Daily temperature reanalysis dataset is global and covers eleven depths (0, 25, 50, 75, 100, 150, 200, 250, 500, 1000, 2000 m). Temperature data is daily, for the period 01/01/1993 to 31/12/2019. Biodiversity data are global and species richness was estimated for the same eleven depths as temperature.
Data exclusions	No data were excluded.
Reproducibility	Data used are open access and detailed R code scripts are provided (Figshare; DOI: 10.6084/m9.figshare.19174985) to ensure the reproducibility of the study.
Randomization	Not applicable.
Blinding	Not applicable.

Did the study involve field work?   ☐ Yes   ☒ No

Reporting for specific materials, systems and methods

We require information from authors about some types of materials, experimental systems and methods used in many studies. Here, indicate whether each material, system or method listed is relevant to your study. If you are not sure if a list item applies to your research, read the appropriate section before selecting a response.

Materials & experimental systems

n/a	Involved in the study
☒	☐ Antibodies
☒	☐ Eukaryotic cell lines
☒	☐ Palaeontology and archaeology
☒	☐ Animals and other organisms
☒	☐ Human research participants
☒	☐ Clinical data
☒	☐ Dual use research of concern

Methods

n/a	Involved in the study
☒	☐ ChIP-seq
☒	☐ Flow cytometry
☒	☐ MRI-based neuroimaging